Research Paper

Holocene coral reef development in Chenhang Island, Northern South China Sea, and its record of sea level changes

Yifang Ma [a,1], Yeman Qin [a,1], Kefu Yu [a,b,*], Yinqiang Li [a], Yating Long [a], Rui Wang [a], Tianlai Fan [a], Wei Jiang [a], Shendong Xu [a], Jianxin Zhao [c]

[a] Guangxi Laboratory on the Study of Coral Reefs in the South China Sea, Coral Reef Research Center of China, School of Marine Sciences, Guangxi University, Nanning 530004, China
[b] Southern Marine Science and Engineering Guangdong Laboratory (Zhuhai), Zhuhai 519080, China
[c] Radiogenic Isotope Facility, School of Earth and Environmental Sciences, The University of Queensland, Brisbane, QLD 4072, Australia

ARTICLE INFO

ABSTRACT

Holocene coral reef development is valuable to understanding the behavior and impacts of paleoclimate and sea level changes. This study focuses on the Holocene carbonate sequences of a drill core extracted from Well CK2 in the northern South China Sea (SCS). This drill core consists of an 873.55 m thick carbonate layer overlying 55.20 m of volcanic basement. High precision U-series dating of 22 coral samples suggests that the Holocene coral reef, which has a thickness of 16.7 m, initiated at ~7800 yr BP (years before 1950 CE) and stopped vertical accretion at 3900 yr BP. The mean vertical accretion rate in the Holocene in Well CK2 was 3.48 m kyr^{-1}, varying from 6.44 m kyr^{-1} during 7800–6000 yr BP to 0.87 m kyr^{-1} during 6000–3900 yr BP. After 3900 yr BP, the vertical development of the reef ceased, indicating that the reef development likely involved lateral accretion. The Holocene section mostly consists of unconsolidated coarse sediments, mainly including corals, coralline algae, large benthic foraminifera, and mollusks. Based on the relationship between coral reef development and sea level, together with the age profile, we determined that the relative sea level near Chenhang Island rose rapidly between 7800 and 6000 yr BP, slowed at ~6000 yr BP, and reached a position of about 2 m above the present-day mean sea level by 3900 yr BP. After 3900 yr BP, the sea level was stable or fell, resulting in a cessation in the reef's upward development.

1. Introduction

Coral reefs are valuable archives of information on the environmental status. They are highly sensitive and their development is of great significance to recording global temperature changes, abrupt climate changes (Damassa et al., 2006; Yu et al., 2010), the intensity of ENSO events (Dang et al., 2020; Jiang et al., 2021; Woodroffe et al., 2003), and sea level fluctuations (Yu and Zhao, 2010; Yu et al., 2009). The timing of the reef initiation, the thickness, and the accretion rate of coral reefs are influenced by the relative changes in sea level (Braithwaite et al., 2000; Webb and Kench, 2010). Using the development of coral reefs to reconstruct the sea level can provide an important and long-term perspective for understanding the development of reefs under sea level change and the study of sea level rise and fall (Woodroffe and Webster, 2014).

Increasing attention has been paid to the relationship between coral reef development and sea level change over the past 40 years. As a driving force or limiting factor, sea level changes affect the development patterns of coral reefs (Saunders et al., 2016). Six growth coral reef patterns have been described in previous studies, which correspond to sea level changes (Davies and Montaggioni, 1985; Woodroffe and Webster, 2014). 1) The "drowned give-up stage": the rate of the coral reef accretion is much slower than the rate of sea level rise, so water depth above the reef increases until it becomes too deep to support reef development. 2) The "backstepped give-up stage": the rate of the sea level rise slows down and the reef retreats shoreward. 3) The "keep-up stage": the reef's accretion rate keeps pace with the rate of sea level rise. 4) The "catch-up stage": the vertical accretion rate of a reef that had not previously been keeping up with the more rapid sea level rise gradually accelerates after sea-level stabilization. 5) The "prograded stage": a reef

---

that had previously been keeping up with sea level can no longer develop vertically after the sea level stabilizes, so it accumulates laterally instead. 6) The "emergent give-up stage": the reef ceases to develop or even becomes exposed as a result of a continuing decline in sea level. What the above models of coral reef development all reflect is a potential response to changes in sea level. Sea-level curves have been reconstructed from preserved coral reefs in the Indo-Pacific region in several studies (Woodroffe and Horton, 2005). However, research on the evolution of coral reefs and sea level reconstruction remains controversial due to the confounding influences of numerous factors on reef development, including large-scale differences in environmental conditions (Macintyre et al., 1992), small-scale differences in basal properties (Cabioch et al., 1995), local tectonic activity (Digerfeldt and Hendry, 1987), and the reliability of depth indicators (Hongo and Kayanne, 2010). For example, there was a Middle to Late Holocene hiatus in reef development throughout the East Pacific Ocean due to ENSO variability (Toth et al., 2017). Additionally, the initial timing of reef development and the thickness of the coral reef strata vary due to a combination of factors such as the hydrodynamic energy, topography, and developmental substrate (Rees et al., 2006).

In the Quaternary, the pattern of global sea level change has been strongly controlled by the growth and contraction of the ice sheets (Lambeck et al., 2014). During the last interglacial period (128–115 ka), the sea level was close to the present-day mean sea level (MSL), which is suitable for the development of reefs. This is consistent with the results of our study, i.e., that the Holocene coral reefs in Chenhang Island formed in the Late Pleistocene (older than 110 ka). Since the last deglacial period, the Earth has entered a stage of ice retreat, and the sea level has increased overall. In the coastal areas of the world, due to the continuous melting of the polar ice sheets and glaciers (Smith et al., 2011), the eustacy has continued to rise rapidly during this period. As the substrate (often the last interglacial reef limestone) was submerged by sea water due to the rise in sea level, a shallow water environment suitable for coral recruitments and growth and space for growth were formed (Cabioch et al., 1995; Gischler and Hudson, 2019). Then, the

Holocene coral communities colonized the inner shelf substrates (Montaggioni, 2005) and began to accrete vertically to a certain thickness as sea level rose. This cumulative thickness indicates the extent of the sea level change since its development. Numerous sea level reconstructions have shown that there have been distinct regional changes in sea level during the Holocene. The Indo-Pacific sea level history is characterized by a Mid-Holocene RSL highstand (Montaggioni, 2005), after which it stabled or fell due to ocean siphoning (Woodroffe and Webster, 2014). Many reef flats emerged following this fall of sea level. Whereas, in the Middle to Late Holocene the Atlantic sea level has risen continuously to the present-day sea level at a decreasing rate due to reduced meltwater input (Khan et al., 2017) and the siphoning effect of the tropical Atlantic (Dullo, 2005). There is little evidence of a sea-level highstand in the Caribbean (Adey, 1978; Khan et al., 2017; Woodroffe and Webster, 2014). Sea level is spatially variable, so it is crucial to reconstruct regional sea level histories.

Coral reefs are widely distributed in the South China Sea (SCS), where they have an area comparable to those in the Great Barrier Reef (Yu and Zhao, 2009), and they initiated at ~20 Ma (Fan et al., 2020). During the past 40 years, many wells have been drilled to study the evolution of coral reefs in the SCS, including Well Nanyong-1, Well Nanyong-2, Well Xiyong-1, Well Xiyong-2, Well Xichen-1, Well Xishi-1, Well Xishi-2 (Yu and Zhao, 2009), and Well Xike-1 (Shao et al., 2017). Although many deep reef cores have been drilled, the Holocene sections of these cores have not been deeply studied. Well CK2 provided a 928.75 m thick carbonate and basaltic volcanic breccia drill core with a carbonate thickness of 873.55 m and a subduction-related volcanic basement thickness of 55.20 m. It was drilled in 2013 from Chenhang Island, the Xisha Islands, northern SCS (Fig. 1). Previous investigators have studied the chronological framework (Fan et al., 2020; Zhang et al., 2020), diagenesis (Wang et al., 2018), carbon isotopes and carbon cycling (Xu et al., 2019), elemental geochemistry, and monsoon activity features (Jiang et al., 2019) of the core from Well CK2. This study focuses on coral reef development based on the Holocene strata in Well CK2 and discusses the inferred sea level changes recorded by the reef
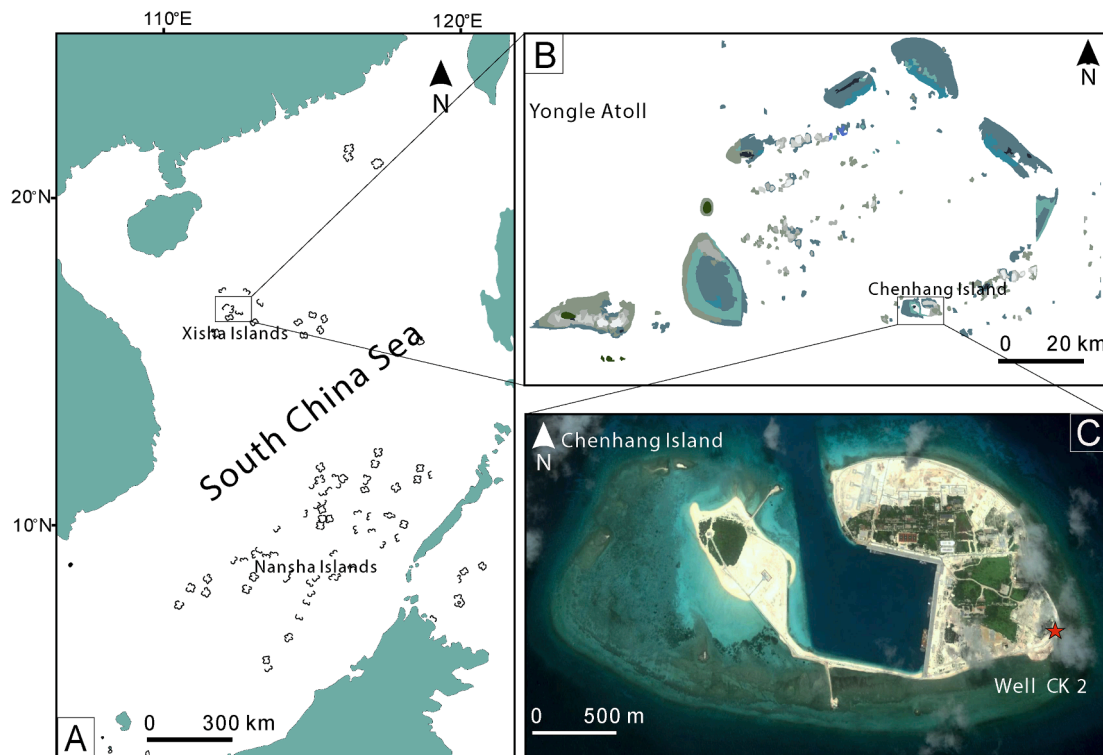

Fig. 1. Maps of the Xisha Islands, Yongle Atoll, and Chenhang Island, showing their location in the South China Sea and the location of the core site. (A) Site of the Xisha Islands, South China Sea. (B) Location of Chenhang Island, the Xisha Islands. (C) Location of Well CK2.

development.

2. Study area

Chenhang Island (16°27′ N, 111°43′ E) is located in the southeast of Yongle Atoll in the Xisha Islands (Fig. 1), which consists of a consolidated gravel facies composed of lime-sand islets (Huang et al., 2011a). The instrumental data from the nearby (80 km away) Yongxing Marine Station (Huang et al., 2011b) show that the annual mean sea surface temperature (SST) in the northern Xisha Islands is 27.4 °C, with a minimum temperature of 24.7 °C occurring between December and February and a maximum temperature of 29.8 °C occurring between May and September. The average surface salinity in this area is 33.6‰, ranging from 33.3‰ in October to 33.9‰ in February (Xu et al., 2019). Zhao et al. (2017) evaluated the intercommunity species diversity of Yongle Atoll where Chenhang Island is located. They determined that according to the similarity of the coral species, the coral communities in Yongle atoll fall into three categories: reef slope, reef flat, and lagoon slope. A total of 58 coral species belonging to 9 families and 21 genera were recorded at Chenhang Island, and among them, *Acropora*, *Favia*, *Porites*, and *Pocillopora* are common genera.

3. Material and methods

The core was drilled from Chenhang Island in the southeastern corner of the lime-sand islets, 2.9 m above the modern reef flat. The core is 873.55 m thick and has an average recovery rate of 70%. In-situ coral branches with a well-preserved skeletal structure are ideal dating materials for obtaining accurate ages. Twenty-two well-preserved *Acropora* spp. samples were taken from the upper 21.40 m of the core to reconstruct a detailed chronostratigraphy of the Holocene coral reef (Fig. 2). In a previous study conducted by Fan et al. (2020), the lithological characteristics and mineralogy of Well CK2 were examined via microscopic observations of 300 thin sections under a polarizing microscope. X-ray diffraction (XRD) analysis was also conducted to determine the mineralogical composition and diagenetic changes within the samples. Their results indicate that the 21.40–0 m core from Well CK2 is mainly composed of a mixture of coral debris, containing aragonite and high-magnesium calcite. The sample selection and treatment methods used were similar to those used in previous studies (Yu et al., 2006). *Acropora* spp. branches with well-preserved skeletal surface structures in the investigated section were selected as the dating samples. First, these samples were sliced to remove any surface calcium scaling, were ultrasonically oscillated in distilled water to remove debris particles, were dried at 50 °C, and were sealed in plastic bags. The U-Th ages of the samples were determined using the Nu plasma multi-collector inductively coupled plasma mass spectrometer (MC-ICP-MS) at the University of Queensland (Clark et al., 2014; Leonard et al., 2018). The MC-ICP-MS technique allows for the accurate determination of the isotopic ratios and concentrations of uranium and thorium with an accuracy of ± 1–2‰ (2σ). The ages are reported as calendar years before present (yr BP), where the present is defined as 1950 CE.

A total of 21 samples were selected from the same section of 21.4 m section of the core for particle size analysis and biological composition analysis. Specific sampling information is provided in Table 1 in the Supporting Information. As has been described by McManus et al.
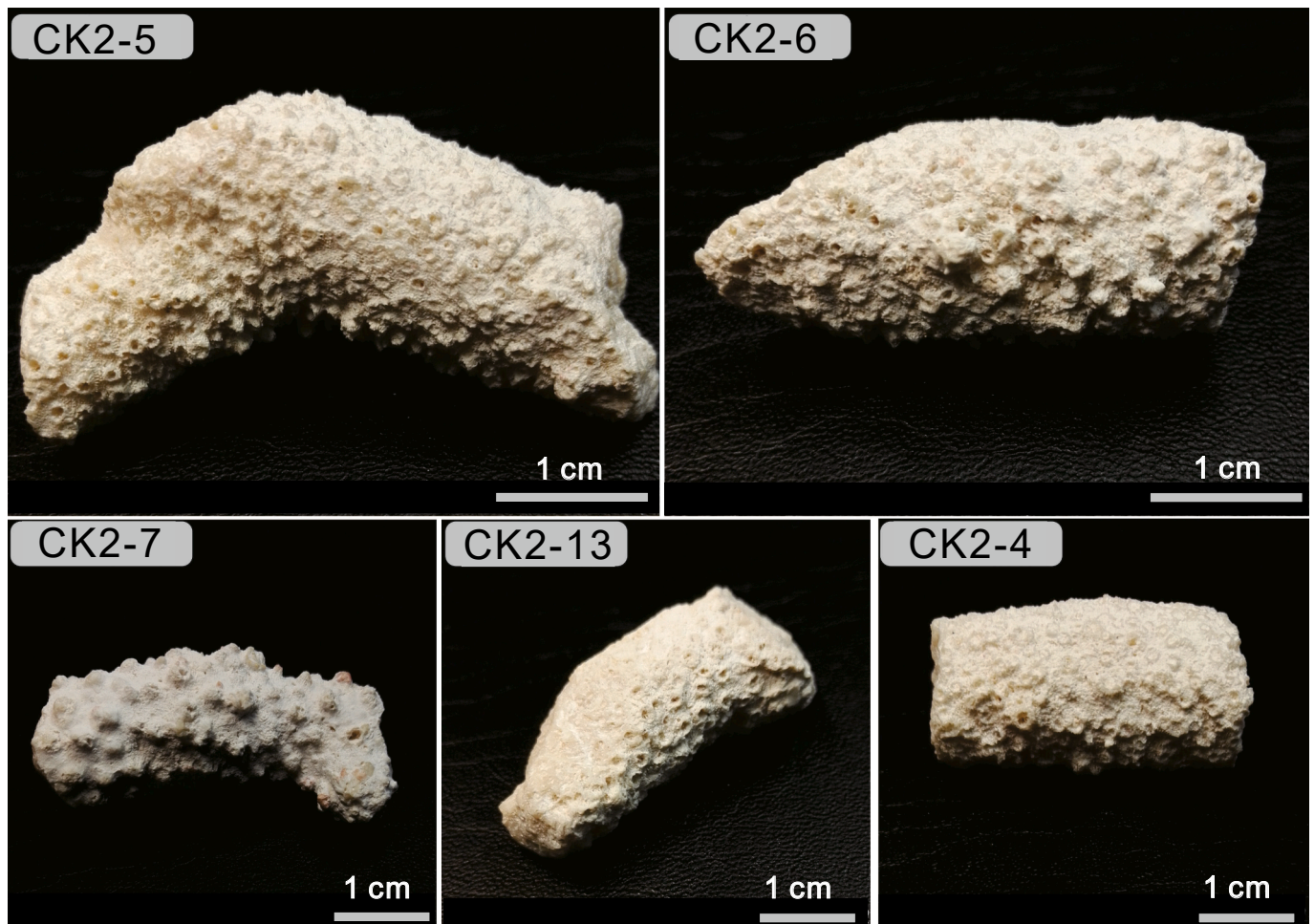

Fig. 2. Photographs of several coral samples used for the dating: samples CK2-4, CK2-5, CK2-6, CK2-7, and CK2-13.

(1998), the grain size analysis was carried out using dry sieving to determine the structural characteristics of the sediments. After the sediment was washed several times with ultra-pure water and then dried at 40 °C, the samples were sieved through a series of graded sieves (including 2000 μm, 1000 μm, 500 μm, 250 μm and 125 μm meshes), and the mass fractions of the sediments with different particle sizes were calculated using the weighing method. The mean grain size (M_z), sorting coefficient (S_d), skewness (S_k), and kurtosis (K_u), were obtained. The mean grain size represents the average grain size. The sorting coefficient (as a standard deviation) refers to the uniformity of the sediment. The skewness measures the asymmetry of the size distribution curve. The kurtosis is a measure of the peakedness of the distribution. The sediments that were 1000–2000 μm in size were removed using ultrasonic oscillation in distilled water, were oven-dried at 40 °C, and were placed in petri dishes. The petri dishes were placed on colored cardboard labeled with numbers. The sediment particles were identified under a binocular stereo microscope; and about 400 sample particles in 45 grids were counted. The biological assemblages of the sediments were divided into the following categories: corals, coralline algae, *Halimeda*, foraminifera, and mollusks.

4. Results

4.1. Chronostratigraphy

The U-Th dating results of the branching coral samples analyzed in this study are summarized in Table 1. The U concentrations (2.9–3.8 ppm) of the upper 17 samples suggest negligible diagenesis (Leonard et al., 2020). The ^{230}Th/^{232}Th ratios range from 92 to 6672, and the data of some of the samples are relatively high, which could be indicative of detrital ^{232}Th. The δ^{234}U values range from 144.5 to 148.6. These values are similar to a previously published range, which was concluded to reflect modern seawater (Shen et al., 2008). This supports the interpretation that the reef aragonite was still in a closed system and the selected coral samples have not undergone diagenesis. The ages of the samples dated in this study vary from 3900 to 7800 yr BP. The oldest sample (depth of 14.2 m) is 7800 yr BP in age and the youngest sample (located at the top of Well CK2, depth of 0.6 m) is 3900 yr BP. Since the initial ^{234}U/^{238}U values of the bottom samples (16.7–20.1 m depth in the core) deviate from the diagenesis indicator of typical seawater values, we used an open-system model to calculate and correct for the age of the open-system corals (Thompson et al., 2003), which revealed that they were deposited during the last interglacial period. The deviation of the sample at the bottom was the largest. The sample's initial ^{234}U/^{238}U was 1.2087 (>1.147). It should be noted that the uranium contents of the five samples at the bottom are much lower than the average value of 3.3 ppm for the Holocene samples, which means that the aragonite was likely transformed into calcite during the Pleistocene and that diagenesis led to the loss of some of the uranium.

The dating results clearly demonstrate the feasibility of the establishment of a precise and accurate chronology for the Holocene deposits based on U-series dating of coral branches, but there are some age-reversals in the data. For example, samples CK2-16 and CK2-17 were both younger than sample CK2-15. Sample CK2-15 was well-preserved, and no traces of encrustation or erosion were observed. It is inferred that samples CK2-16 and CK2-17 should have been located above sample CK2-15. There are two possible reasons for this inversion: 1) sample caving or sample displacement may have occurred during the coring process, resulting in chronological reversal (Johnson and Risk, 1987); and 2) there could have been minor unrecognized diagenesis in some of the samples.

Therefore, in the subsequent establishment of the age framework and calculation of the accretion rate, the selection of the age data was based on the order from the youngest to the oldest, and a total of 11 data points were selected from sample CK2-1 at the top of the core to sample CK2-15 at the bottom of the core. The age reversed samples (CK2-4, CK2-5, CK2-

10, CK2-14, CK2-16, and CK2-17) are regarded as having fallen from the upper strata so that they are discarded. In the development of hypothetical minimum sea level records, we included all 17 Holocene *Acropora* spp. samples.

4.2. Lithology

The analysis of the particle size and biological assemblages of the 21 samples revealed that the mean grain size is 0.66 ϕ (coarse sand). This shows that the sediments may have been deposited in a shallow water medium to high energy sedimentary environment, which as characterized by strong hydrodynamic forces and a large particle size. Most of the samples are poorly sorted (average 1.53), and asymmetrical (average 0.34). The overall kurtosis is medium (average 1.20). This indicates that the particle size distribution is dispersed, the samples are predominantly coarse-grained sediments, and the frequency of the main particle size is not sharp or obtuse. The sediments from the 21 samples range from sand to sandy gravel (−0.54 to 2.55 ϕ). Samples 9, 10, 11, and 12 (M_z of 2.30 ϕ, 1.62 ϕ, 2.55 ϕ, and 2.05 ϕ, respectively) were dominated by fine sand. These samples also had the smallest sorting coefficients (S_d of 1.16, 1.33, 0.88, and 1.25, respectively) and skewness values (S_k of −1.02, −0.69, −1.08, and − 0.91, respectively). The main particle type is coral, with *Acropora* spp. accounting for 59.35% of the entire core. The entire core was divided into three parts with respect to the organic composition of the debris samples. Collectively, these three sections are composed of the same groups of constituents, mainly coral and coralline algal fragments (Fig. 3).

(1) The 0.2–2.1 m and 7.95–10.2 m segments. A prominent feature of these two sections is the high proportion of coral gravels and coral branches with lengths of up to 7 cm. In other words, there are fewer finer grained deposits. A portion of the coral branches are coated with calcareous red algae. The shell fragments, including *Tridacna* are remarkably well-preserved in the upper strata (0.2–2.1 m).

(2) The 2.1–6.95 m and 11.2–16.85 m segments. These sediments are medium-grained sand deposits with gravel inclusions. The skeletal composition is dominated by coral (61.63%) and coralline algae (27.95%), with mollusks contributing approximately 2.35% to the deposits. The foraminifera, *Halimeda,* and other components comprise 0.51%, 4.88%, and 2.66% of the sediments, respectively.

(3) The 6.95–7.95 m and 10.2–11.2 m segments. The major sediment constituents found in this unit, in decreasing order of overall abundance, are coral (48.88%), mollusks (18.36%), other components (14.22%), and coralline algae (11.83%). Foraminifera and *Halimeda* are rare (< 5%). Textural analysis of the sediments indicates that the mean grain size (M_z) reaches a maximum in these two sections. The sorting of the sediments in these sections is generally better than in the other units.

5. Discussion

5.1. Division of the Holocene sedimentary facies in Well CK2

To evaluate the sedimentary facies of reefs, Henson (1950) developed the reef-complexes model which classifies reefs according to their macroscopic shapes, including distal collapse facies, proximal collapse facies, reef slope facies, reef framework facies, reef crest facies, reef flat facies, reef sand facies, and lagoon facies (Luo et al., 2018). Based on field investigations in the Xisha Islands, especially Yongle Atoll, the modern reef sedimentary facies can usually be divided into reef framework facies, reef crest facies, lime-sand islet sedimentary facies, fore-reef collapse facies, and backreef lagoon facies (Wang et al., 1982). To identify the changes in the sedimentary facies in drilling cores, it is necessary to fully understand the sedimentary characteristics of reef-

Table 1

U-Th isotopic compositions and ^{230}Th ages for the fossil coral samples from Chenhang Island obtained using MC-ICP-MS.

Sample name	Material: Coral	Depth (m)	U (ppm)	(^{230}Th/^{232}Th)	(^{234}U/^{238}U)	±2σ	(^{230}Th/^{238}U)	±2σ	Uncorr. ^{230}Th Age (yr)	±2σ	Corr. ^{230}Th Age (yr)	±2σ	Calendar age (cal yr BP)	δ^{234}U	±2σ
CK2-1	*Acropora* spp.	0.6	2.9514	91.93	1.1442	0.0010	0.04155	0.00026	4036	26	4001	31	3933	145.9	1.0
CK2-2	*Acropora* spp.	1.2	3.3216	768.21	1.1456	0.0007	0.04992	0.00033	4860	33	4855	33	4787	147.6	0.7
CK2-3	*Acropora* spp.	2.4	3.4893	1380.90	1.1439	0.0008	0.06206	0.00033	6084	34	6081	34	6013	146.4	0.9
CK2-4	*Acropora* spp.	2.8	3.0350	1838.50	1.1448	0.0008	0.06009	0.00026	5881	27	5879	27	5811	147.2	0.8
CK2-5	*Acropora* spp.	3.7	3.0789	2143.58	1.1454	0.0007	0.06003	0.00033	5872	33	5870	33	5802	147.8	0.7
CK2-6	*Acropora* spp.	4.7	3.1050	411.02	1.1459	0.0014	0.06681	0.00058	6542	59	6529	59	6461	148.6	1.5
CK2-7	*Acropora* spp.	4.9	3.1543	329.37	1.1451	0.0008	0.07016	0.00030	6896	30	6879	31	6811	148.0	0.8
CK2-8	*Acropora* spp.	5.2	3.8261	6672.47	1.1446	0.0008	0.07079	0.00033	6963	34	6962	34	6894	147.4	0.8
CK2-9	*Acropora* spp.	6.6	3.0566	183.05	1.1431	0.0010	0.07247	0.00038	7143	39	7112	42	7044	146.0	1.0
CK2-10	*Acropora* spp.	7.5	3.5221	4601.40	1.1444	0.0008	0.07121	0.00036	7006	37	7005	37	6937	147.3	0.8
CK2-11	*Acropora* spp.	8.7	3.2702	921.63	1.1443	0.0007	0.07534	0.00033	7427	34	7421	34	7353	147.4	0.7
CK2-12	*Acropora* spp.	9.3	3.0095	121.48	1.1445	0.0007	0.07787	0.00032	7684	33	7633	41	7565	147.7	0.7
CK2-13	*Acropora* spp.	12.5	3.5334	2110.60	1.1422	0.0009	0.07777	0.00048	7690	49	7687	49	7619	145.4	0.9
CK2-14	*Acropora* spp.	13.0	3.6084	5351.56	1.1441	0.0012	0.07774	0.00049	7674	50	7672	50	7604	147.3	1.3
CK2-15	*Acropora* spp.	14.2	3.4340	1638.75	1.1429	0.0016	0.08004	0.00065	7917	67	7914	67	7846	146.1	1.6
CK2-16	*Acropora* spp.	14.4	3.2884	485.73	1.1453	0.0015	0.07675	0.00070	7564	72	7552	73	7484	148.5	1.5
CK2-17	*Acropora* spp.	16.1	3.5734	1457.51	1.1414	0.0012	0.07672	0.00053	7588	55	7584	55	7516	144.5	1.3
CK2-18	*Acropora* spp.	16.7	1.2630	12,159.72	1.1123	0.0019	0.72657	0.00216	112,700	700	112,700	700	112,632	154.4	2.5
CK2-19	*Fungia* spp.	17.6	0.9928	53.36	1.1114	0.0014	0.78386	0.00265	129,200	900	128,100	1000	128,032	161.9	2.2
CK2-20	*Acropora* spp.	18.8	1.5819	329.91	1.1115	0.0013	0.81605	0.00295	139,600	1100	139,400	1100	139,332	165.6	1.8
CK2-21	*Acropora* spp.	19.6	2.1799	570.04	1.1105	0.0014	0.83109	0.00341	145,100	1300	144,900	1300	144,832	166.6	1.9
CK2-22	*Acropora* spp.	20.1	1.3335	99.07	1.1270	0.0018	0.91903	0.00284	173,800	1500	173,100	1500	173,032	208.7	2.8

*The ratios in parentheses are activity ratios calculated from the atomic ratios based on the decay constant published by Cheng (2000). Errors are at 2σ level for the least significant digits. The ages were calculated using ^{230}Th and ^{234}U half-lives of 75,380 and 244,600 years, respectively. Corr. and uncorr. denote corrected and uncorrected, respectively. The corrected ^{230}Th ages and initial (^{234}U/^{238}U) ratios include a negligible to small correction for initial/detrital U and Th (Clark et al., 2014), which was conducted using an average crustal ^{232}Th/^{238}U atomic ratio of 3.8 ± 1.9 (^{230}Th, ^{234}U, and ^{238}U were assumed to be in secular equilibrium). δ^{234}U = [(^{234}U/^{238}U)-1] × 1000. All of the U-series ages (yr BP) are relative to 1950 CE.
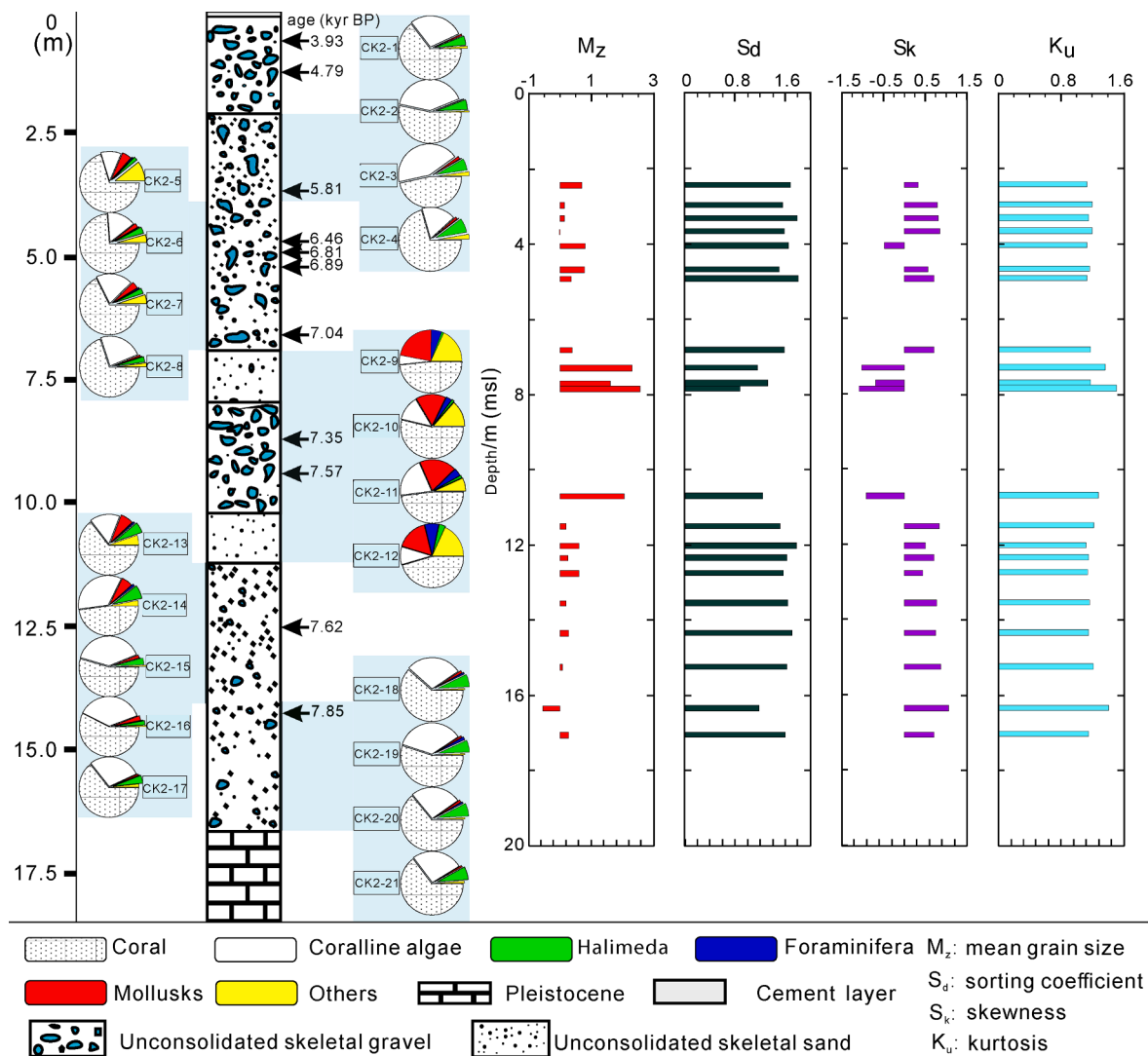
Fig. 3. Sedimentary log of the core and the locations of the U-Th dated samples. The inferred growth isochrones are in calendar years BP and are based on dated intervals within the core. The vertical transitions in the reef facies are based on changes in the framework fabrics and the composition of the sedimentary matrix. The relative abundances of the bioclastic components are presented as pie charts. The grain size parameter is shown on the right.

building organisms. The facies of the upper 16.85 m of the core were determined to be characterized by unconsolidated bioclastic limestone and coral rubble based on analysis of the core lithology. The dominant biological assemblages were branching genus *Acropora*, mollusk fragments, and benthic foraminifera. The Holocene sedimentary environment of Well CK2 was the lime-sand islet sedimentary facies, which is equivalent to the reef flat facies and backreef sand facies of the reef complex model.

The 0.2–2.1 m and 7.95–10.2 m sections in Well CK2 are dominated by branching corals, mollusk gravel, bivalves, and coralline algae which are supported by a small amount of sandy matrix. The 2.1–6.95 m and 11.2–16.85 m sections are supported by more bioclastic matrix which is chiefly coarse-sand sized, including foraminifera, molluscs, corallines debris, *Halimeda* plates, alcyonarian spicules, echinoid detritus, and brachiopods. All of them can be defined as skeletal rubble facies (Montaggioni, 2005). It is unconsolidated and may be supported by a sandy matrix. The facies may occupy up to 60% of the total core volume (Davies and Hopley, 1983; Grossman and Fletcher, 2004; Kennedy and Woodroffe, 2000; Montaggioni, 1988) and are usually deposited at the surface of reef flats and prograde into the backreef zone (Davies and Hopley, 1983). According to these findings, the 0.2–6.95 m, 7.95–10.2 m, and 11.2–16.85 m sections are inferred to be reef flat facies, and the

sedimentary environment was an inner reef flat. The inner reef flat is gently sloped from the reef toward the lagoon, there was less influence from the waves and more sand debris in the tidal ditch and reef pit.

The grain sizes of the 6.95–7.95 m and 10.20–11.20 m sections are finer than those of the other intervals, the content of corals and coralline algae decreases, while the contents of mollusks, foraminifera, and unidentified species increase. The reef should be located on the inner reef flat or on the lagoon slope, showing the characteristics of the backreef sand facies and a relatively low-energy environment (Kench and Brander, 2006), and the depth of the water at this time was slightly deeper than that in other periods. This phase is defined as the carbonate sand facies, which is also known as skeletal, detrital, biogenic, or bioclastic sand (Montaggioni, 2005). The skeletal sand facies is widespread beneath a variety of reef zones, is mainly distributed on the inner reef flat and backreef, and the volume of the sand accounts for more than 80% of the total core volume (Cabioch et al., 1999; Davies and Hopley, 1983; Marshall and Davies, 1982). According to these findings, the 6.95–7.95 m and 10.20–11.20 m sections are inferred to be backreef sand facies.

5.2. Initial age of the Holocene coral reef in Well CK2 and its sea level significance

Many previous studies have provided sufficient information on the evolution of the various coral reef systems in the Indo-Pacific Ocean (Grossman and Fletcher, 2004; Smithers et al., 2006). However, the coral reefs in Southeast Asia, especially in the SCS, remain poorly studied in terms of Holocene coral reef evolution and sea level reconstruction. The U-Th results for Well CK2 (Table 1) provided precise age framework for the development of the Holocene coral reefs in the SCS. Since the low $^{234}U/^{238}U$ value (1.1123) suggests open-system behavior, and the corrected age (112 ka) is also from the last interglacial period, sample CK2-18 is definitely the upper boundary of the Pleistocene section of the reef. The initial development time of the Holocene coral reef in Chenhang Island was 7800 yr BP. Compared with the thickness and time (Fig. 4), our results are basically in agreement with global Holocene coral reef development. Most of the Holocene reefs in the Indo-Western Pacific, Central Pacific and Caribbean have ages of 8300–7000 yr BP (Montaggioni, 1988). The onset of Holocene reef development varied from 9600–8000 yr BP in the Indian Ocean, 9860–1660 yr BP in the Pacific Ocean, and 9400–6000 yr BP in the Caribbean. Consequently, the initial development time of most coral reefs in the Early Holocene (concentrated at 9000–7000 yr BP) and their high growth potential were mainly driven by the position of the initiation surface relative to sea level (Dullo, 2005; Hongo, 2012).

The substrate of the Holocene coral reef of Chenhang Island was the reef developed during the last interglacial period. Therefore, we conclude that the coral reef stopped growing at the end of the last interglacial period, remained in a stagnant state until the sea level rose again to a suitable position for coral growth at (i.e., ~7800 yr BP), and then the reef began to develop vertically up until it reached a thickness of 16.7 m. The tectonic activity in the SCS has been relatively stable during the Holocene. The subsidence rate of Chenhang Island is 0.07–0.1 mm yr^{-1} (Zhao, 1998; Zhao et al., 1999), indicating that the impact of subsidence on the Holocene coral reefs has been negligible. The modern reef flat level is roughly the same as the MSL in Chenhang Island, and the drilling position of Well CK2 is about 2.9 m above the modern reef flat. The modern reef flat of Chenhang Island is defined as having a relative elevation of 0 m. The initial development age of the

Holocene reef in Chenhang Island (at a depth of 14.2 m in the core, or at 11.3 m below the modern reef flat) recorded that the RSL in the northern SCS was already at or above −11.3 m by 7846 ± 67 yr BP.

5.3. Well CK2 accretion rate and its implications for Holocene sea level fluctuations

From 7800 yr BP to 3900 yr BP, the average accretion rate of the reef on Chenhang Island was 3.48 m kyr^{-1}, with vertical accretion rates of 6.44 m kyr^{-1} from 7800 to 6000 yr BP and 0.87 m kyr^{-1} from 6000 to 3900 yr BP. The vertical accretion rate from 7800 to 6000 yr BP can be further subdivided into 17.48 m kyr^{-1} (7846–7565 yr BP), 5.83 m kyr^{-1} (7565–6811 yr BP), and 3.13 m kyr^{-1} (6811–6013 yr BP). Based on the variations in the Holocene development sequences and the accretion rate of the reef in Well CK2, we drew a depth-age curve (Fig. 5A) and reconstructed the developmental history of the section in Well CK2 from 7800 to 3900 yr BP. We found that the accretion rate of the reef in Well CK2 gradually decreased during the Holocene. There was an obvious decrease in the accretion rate from 17.48 m kyr^{-1} (7846–7565 yr BP) to 5.83 m kyr^{-1} (7565–6811 yr BP). It is more likely that the change in the accretion rate of the coral reefs was the result of changes in sea level relative to the accommodation of the reefs, and the reef may have been developed nearly at sea level at this time. The sea level records reconstructed based on the coral reef accretion rate curve for Well CK2 reveal the sea level fluctuations in the Holocene.

We selected *Acropora* spp. as the dating samples in order to represent the paleo-sea level as well as possible. The depth and age data for the coral samples were used as sea level indicators. However, the depth of the coral should be considered as the location of the minimum sea level. The paleo-sea level may actually have been a few meters higher than the depth at which the coral grew at that time. The RSL record for Chenhang Island shows that the sea level record is characterized by a rapid rise in sea level between 7800 and 6800 yr BP, followed by a decreasing rate at ~6000 yr BP, at which time it reached the present-day MSL. After this, the rate of sea level rise decreased. Finally, the sea level stabilized at about 2 m above the present-day MSL by 3900 yr BP (Fig. 5B).

During the early Holocene, the sea level rose in most parts of the world due to the meltwater released (Smith et al., 2011; Woodroffe and Horton, 2005). The Holocene RSL records show that spatio-temporal
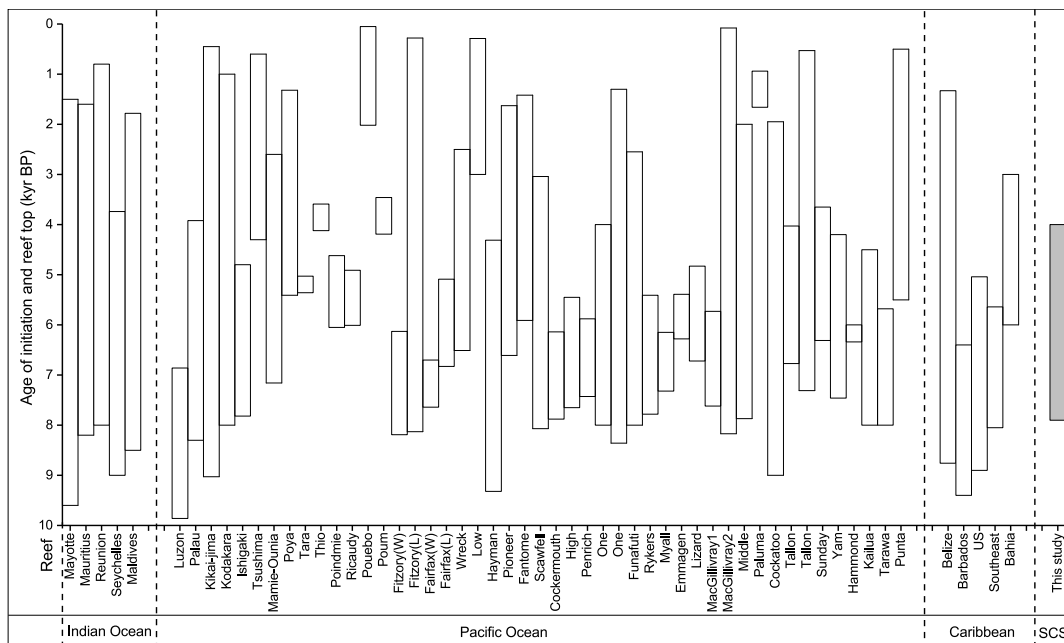

Fig. 4. Summary of the initiation and reef top times of the several Holocene reefs (modified from Qin et al. (2019)). The Holocene initiation and reef top time data for 57 reefs are summarized. W stands for windward; L stands for leeward. 1 and 2 represent two sets of time data for the reef.
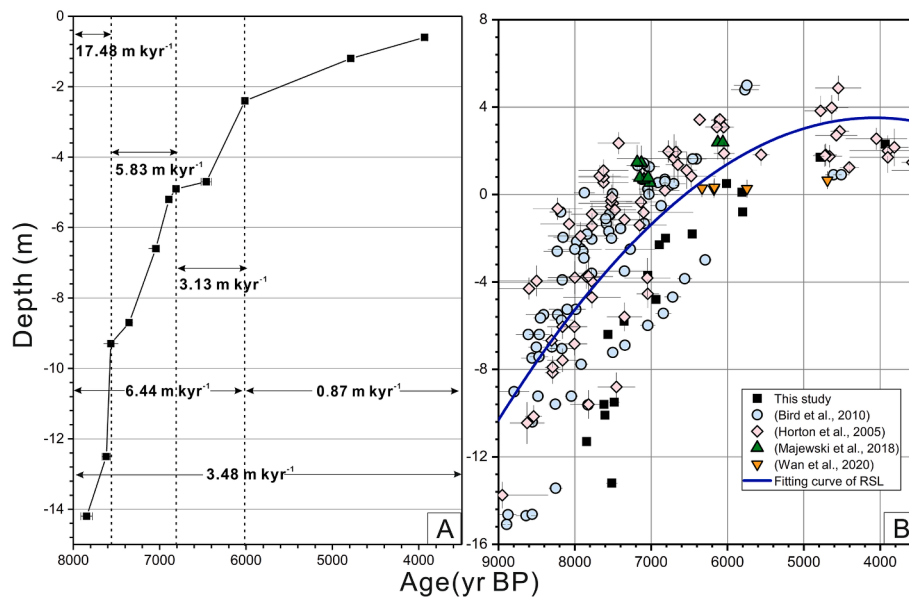
Fig. 5. (A) Depth vs. age plots of fossil corals in core CK2. Depths are relative to the wellhead depth. (B) Comparison of the sea-level records for Chenhang Island, Natuna Island (Wan et al., 2020), Western Borneo (Majewski et al., 2018), and the datasets for Singapore (Bird et al., 2010) and the Malay-Tai Peninsula (Horton et al., 2005). The errors in the ages and depths are indicated by the lengths of the crossbars.

variability (Khan et al., 2017; Khan et al., 2015). A Mid-Holocene highstand is the main characteristic of the Middle to Late Holocene RSL in the far-field (Lambeck et al., 2014; Mitrovica and Milne, 2002). The datasets for the Malay-Thai Peninsula confirm the upward trend of the RSL in the Holocene to a Mid-Holocene highstand. In the Malay-Thai Peninsula, the RSL rose to a maximum of 4.87 ± 0.57 m at 4850–4450 yr BP, with an average rate of sea-level rise of 5.5 m kyr^{-1} (Horton et al., 2005). Conversely, the datasets for Singapore show that the rise in the RSL was discontinuous throughout the Holocene. In Singapore, the sea level records suggest a rapid rise at a rate of 18 m kyr^{-1} until 8100 yr BP, an intermission period at 7800–7400 yr BP, followed by a renewed rise of 4–5 m that was complete by 6500 yr BP (Bird et al., 2010). The initial rate of sea level rise (18 m kyr^{-1} in 8800–8100 yr BP) in Singapore was similar to the rapid rise rate of the reefs in Chenhang Island. In the Early Holocene, the sea level at Chenhang Island, rose rapidly, increasing by nearly 5 m from 7800 to 7600 yr BP at a rate of about 17.48 m kyr^{-1}. Then, the rapid sea level rise was over by 6000 yr BP. Similar to the early period of the RSL stability in Singapore, the data for western Borneo suggest that the rapid RSL rise was over by 7450 yr BP (Majewski et al., 2018). The temporal differences in these rapid RSL rise endpoints could be caused by the spatial variability of the rheology of the Sunda Shelf (Majewski et al., 2018).

In Natuna Island, which is located between northwestern Borneo and eastern Malaysian Peninsula, the high-precision RSL record over the past 6400 years, indicate that the RSL was relatively stable from 6400 to 1400 yr BP and was 0.2–0.7 ± 0.4 m higher than present (Wan et al., 2020). The rapid sea level rise was not been recorded. The data for Western Borneo, which is geographically similar, suggest that the sea level highstand at 6000–6100 yr BP was 2.38 m higher than the present-day MSL (Majewski et al., 2018). In the same period, the RSL recorded in Chenhang Island in the Xisha Islands was 0.5 m higher than the present-day MSL. Although the RSL recorded in Western Borneo and Natuna Island, which are within 1600 km of the Xisha Islands, and the RSL in Chenhang Island had all exceeded the present-day MSL by ~6000 yr BP, there were differences in the height of the Mid-Holocene RSL highstand in these locations, which were most likely caused by hydro-isostatic processes (Horton et al., 2005; Zong, 2004). It is likely that the spatial variations in the sea level at these localities was predominantly due to the influence of the ice and ocean mass redistribution on sea-level change (Milne et al., 2005). The eustatic sea level (ESL) rise from ice

melting had largely ceased by 6000 yr BP (Argus et al., 2014). The later rise at these locations was the result of Glacial Isostatic Adjustment (GIA) and equatorial siphoning (Khan et al., 2015; Lambeck et al., 2014). Numerous precious studies have shown that these models are constantly being updated, such as the ICE-6G (Peltier et al., 2018; Toscano et al., 2018) and ICE-7G models (Roy and Peltier, 2015, 2017). The changes in the ESL can be estimated using the reconstructions of GIA models.

The RSL fitting curve suggests that the rate of sea level rise gradually decreased in the Early Holocene, and the reefs in Chenhang Island gradually approached sea level, limiting the space for accommodation, which is consistent with the gradually decreasing reef development rate indicated by the reef age curve. However, the record of the minimum RSL for Chenhang Island differs slightly from the records of rapid sea level rise provided by the Singapore and the Malay-Tai Peninsula datasets (Bird et al., 2010; Horton et al., 2005). This might be the result of GIA. Or, more likely, the sea level could already have been rising rapidly (from deeper depths) by the time the corals started growing at the site of the core from Well CK2. Although a regional single sea level curve cannot accurately summarize the local relative sea level history (Khan et al., 2017), the records in the Southeast Asian region on a long-time scale are basically consistent with our results. Additionally, the accretion history of Well CK2 is synchronous with that of most coral reefs in the world, which verifies the reliability of our reconstruction results. We will focus on the impact of GIA on the sea level change around Chenhang Island future studies to attain a better comparison of our results with other sea level records in other regions of the world.

5.4. The age of the top of Well CK2 and its record of sea level fell/stability at ~3900 yr BP

The U-Th age of the top of Well CK2 (Table 1) is 3933 ± 31 yr BP. The age of the reef top varies greatly in different regions of the world. The drilling cores from One Tree Reef in the Great Barrier Reef in the western Pacific Ocean vary in age from 1315 ± 6 to 6008 ± 26 yr BP at the top of reefs (Sanborn et al., 2020). As shown in Fig. 4, the reef top age ranges are 800–3740 yr BP in the Indian Ocean, and 500–6860 yr BP in the Pacific. Regionally, as early as 1979, the coral conglomerate in the SCS was drilled at 20–30 cm below the central surface of Ganquan Island when Lu et al. (1979) studied the Quaternary biodeposition and island

formation in the Xisha Islands. The ^{14}C dates indicate the age is 3400 ± 160 yr BP. Nie (1996) drilled core samples from the top surfaces of primary shore corals on several reef plains throughout the SCS. The radiocarbon dates of their samples revealed that the ages of the surface corals from Dongdao Island and Yongxing Island in the Xisha Islands are 4340 ± 250 yr BP and 3600 ± 90 yr BP, respectively. These findings are in close agreement with the reef top age of 3900 yr BP obtained in this study.

The age of the top of the reef usually indicates a variation in the reef development model during that period, indicating a stagnation in the vertical development of the reef. In accordance with the relationship between coral reef development and sea level summarized above, the main factor encouraging or limiting the growth of biological reefs was the elevation difference between the sea level and the reef, i.e., the accommodation space (Grossman et al., 2006). Our data suggest that the vertical growth stagnated when the Chenhang Island coral reef grew to about 2 m above the present-day MSL at ~3900 yr BP. The reason for this stagnation was likely stabilization of the sea level (i.e., no longer rising or falling) (Smithers et al., 2006). We infer that the sea level had fallen or stabilized at ~3900 yr BP. The sea level at 3900 yr BP would have been at least 2 m (or 2.9 m) higher than the present MSL since the coral elevation represents a minimum sea level.

Mid-Holocene sea-level highstands are widely recorded in the northern SCS (Shi et al., 2007; Shi et al., 2008; Zhao and Yu, 2002). The evidence of coral reefs and their biological-geomorphological zones from Leizhou Peninsula shows five episodes of sea-level highstands during the Holocene, which occurred at 7200–6700 yr BP, ~5800 yr BP, 5000–4200 yr BP, 2800–2000 yr BP, and ~1500 yr BP (Yu et al., 2002). Among them, the highest sea-level stand in the Holocene occurred at 7200–6700 yr BP, which is confirmed by the coral reefs in the Luhuitou area of Hainan Island (Huang et al., 2005). Moreover, the existence of a sea-level highstand in the Mid-Holocene has also been widely recognized in the Indo-Pacific region (Kench et al., 2009; Mann et al., 2019; Pirazzoli et al., 1987; Yamano et al., 2019). A comparative study of the RSL curves for the Leizhou Peninsula in the SCS (Yu et al., 2009) and Belitung Island in Indonesia demonstrated that sea-level highstands

occurred at ~6800 yr BP and ~6590 yr BP (Meltzner et al., 2017). The similarity between these records reflects widespread changes in sea level. Nevertheless, additional minor fluctuations occurred in the SCS, with an intermediate peak at ~6700 yr BP; Meltzner et al. (2017) ascribed this to the complexity of ocean circulation. The above studies mainly concentrated on the Leizhou Peninsula and Hainan Island which are at relatively high latitudes, while our data suggest that there was a sea-level highstand in the Xisha Islands at 6000–3900 yr BP. However, this more specific sea-level highstand episode and its elevation still need to be studied further.

The falling or stabilization of the sea level may lead to lateral development of coral reefs, that is, when the vertical accommodation space provided by the sea level is insufficient, the reef will undergo a lateral seaward transgression (Leonard et al., 2013; Perry et al., 2011). The Holocene coral reef in Chenhang Island, Xisha Islands, initiated at ~7800 yr BP and accreted vertically until ~3900 yr BP. Subsequently, the sea level may have stabilized or fallen, and under such conditions, we speculate that the reef may have transitioned to a lateral transgression (Fig. 6). However, the determination of the specific reef development model also requires the lateral comparison of multiple drill cores from this area.

6. Conclusions

(1) According to the U-Th ages obtained for 22 coral samples from Chenhang Island, we infer that the growth of the Holocene coral reef on Chenhang Island began at about 7846 ± 67 yr BP, which is consistent with the initiation time of the growth of the coral reefs in the western Pacific, the central Pacific, and the Caribbean.

(2) From 7800 to 3900 yr BP, the vertical accretion rate of the coral reef on Chenhang Island was 3.48 m kyr^{-1}, with vertical accretion rates of 6.44 m kyr^{-1} from 7800 to 6000 yr BP and 0.87 m kyr^{-1} from 6000 to 3900 yr BP.

(3) The age of the top of the coral reef on Chenhang Island is 3933 ± 31 yr BP. Since 3900 yr BP, the vertical development of the coral reef has ceased, but it may have continued in deeper areas.
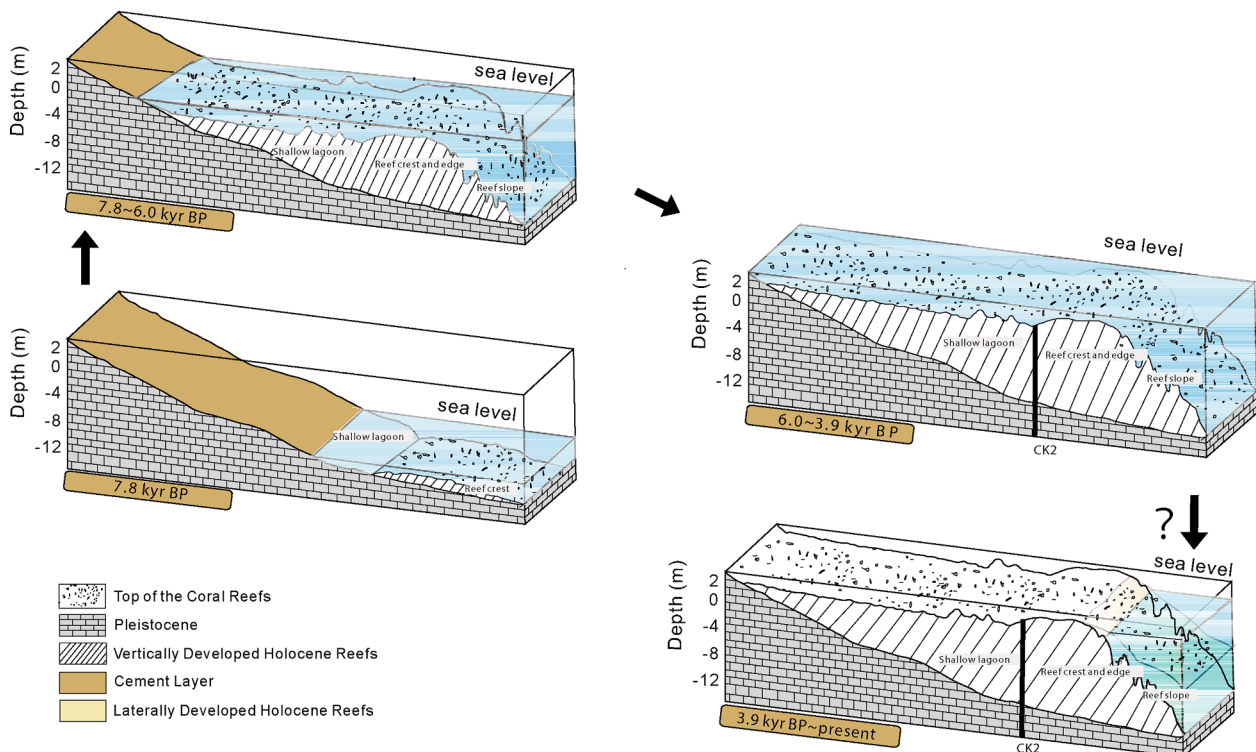

Fig. 6. Schematic diagrams illustrating the speculative growth stages of the reef on Chenhang Island. The depth scale indicates the relative sea level.

(4) According to the relationship between coral reef development and sea level, we conclude that the sea level at ~7800 yr BP was about 11.3 m below the present-day mean sea level. The sea level rose rapidly between 7800 and 6000 yr BP, after which the rate of the sea level rise decreased; and the sea level at ~3900 yr BP rose until it was about 2 m higher than it is today. At ~3900 yr BP, the sea level may have stabilized or fallen gradually, which led to the cessation of the upward development of the coral reefs.

Data availability

The data used in this paper have been deposited in a general data repository; and they are available at https://doi.org/10.6084/m9.figshare.13551668.

Declaration of Competing Interest

This manuscript has not been published or presented elsewhere, in part or in entirety, and is not under consideration by another journal. We have read and understood your journal's policies, and we believe that neither the manuscript nor the study violates any of these. There are no conflicts of interest to declare.

Acknowledgements

Appendix A. Supplementary data

Supplementary data to this article can be found online at https://doi.org/10.1016/j.margeo.2021.106593.

References

Adey, W.H., 1978. Coral reef morphogenesis: a multidimensional model. Science 202, 831–837. https://doi.org/10.1126/science.202.4370.831.

Argus, D.F., Peltier, W.R., Drummond, R., Angelyn, W.M., 2014. The Antarctica component of postglacial rebound model ICE-6G_C (VM5a) based on GPS positioning, exposure age dating of ice thicknesses, and relative sea level histories. Geophys. J. Int. 198, 537–563. https://doi.org/10.1093/gji/ggu140.

Bird, M.I., Austin, W.E.N., Wurster, C.M., Fifield, L.K., Mojtahid, M., Sargeant, C., 2010. Punctuated eustatic sea-level rise in the early mid-Holocene. Geology 38, 803–806. https://doi.org/10.1130/G31066.1.

Braithwaite, C., Montaggioni, L., Camoin, G., Dalmasso, H., Dullo, W., Mangini, A., 2000. Origins and development of Holocene coral reefs: a revisited model based on reef boreholes in the Seychelles, Indian Ocean. Int. J. Earth Sci. 89, 431–445. https://doi.org/10.1007/s005310000078.

Cabioch, G., Montaggioni, L., Faure, G., 1995. Holocene initiation and development of New Caledonian fringing reefs, SW Pacific. Coral Reefs 14, 131–140. https://doi.org/10.1007/BF00367230.

Cabioch, G., Camoin, G., Montaggioni, L., 1999. Postglacial growth history of a French Polynesian barrier reef tract, Tahiti, central Pacific. Sedimentology 46, 985–1000.

Cheng, H., 2000. The half-lives of uranium-234 and thorium-230. Chem. Geol. 169, 17–33. https://doi.org/10.1016/S0009-2541(99)00157-6.

Clark, T.R., Roff, G., Zhao, J.X., Feng, Y.X., Done, T.J., Pandolfi, J.M., 2014. Testing the precision and accuracy of the U–Th chronometer for dating coral mortality events in the last 100 years. Quat. Geochronol. 23, 35–45. https://doi.org/10.1016/j.quageo.2014.05.002.

Damassa, T.D., Cole, J.E., Barnett, H.R., Ault, T.R., McClanahan, T.R., 2006. Enhanced multidecadal climate variability in the seventeenth century from coral isotope records in the western Indian Ocean. Paleoceanography 21, PA2016. https://doi.org/10.1029/2005PA001217.

Dang, S., Yu, K., Tao, S., Han, T., Zhang, H., Jiang, W., 2020. El Niño/Southern Oscillation during the 4.2 ka event recorded by growth rates of corals from the North South China Sea. Acta Oceanol. Sin. 39, 110–117. https://doi.org/10.1007/s13131-019-1520-5.

Davies, P., Hopley, D., 1983. Growth fabrics and growth-rates of Holocene reefs in the Great Barrier-Reef. BMR J. Aust. Geol. Geophysics 8, 237–251.

Davies, P., Montaggioni, L., 1985. Reef growth and sea level change: the environmental signature. Proc. 6th Int. Coral Reef Symp. Antenne Muséum-EPHE 3, 477–511.

Digerfeldt, G., Hendry, M., 1987. An 8000 year Holocene sea-level record from Jamaica: implications for interpretation of Caribbean reef and coastal history. Coral Reefs 5, 165–169. https://doi.org/10.1007/BF00300959.

Dullo, W., 2005. Coral growth and reef growth: a brief review. Facies 51, 33–48. https://doi.org/10.1007/s10347-005-0060-y.

Fan, T., Yu, K., Zhao, J., Jiang, W., Xu, S., Zhang, Y., Wang, R., Wang, Y., Feng, Y., Bian, L., 2020. Strontium isotope stratigraphy and paleomagnetic age constraints on the evolution history of coral reef islands, northern South China Sea. GSA Bull. 132, 803–816. https://doi.org/10.1130/B35088.1.

Gischler, E., Hudson, J., 2019. Holocene tropical reef accretion and lagoon sedimentation: A quantitative approach to the influence of sea-level rise, climate and subsidence (Belize, Maldives, French Polynesia). Depos. Rec. 5, 515–539. https://doi.org/10.1002/dep2.62.

Grossman, E., Fletcher, C., 2004. Holocene reef development where wave energy reduces accommodation space, Kailua Bay, Windward Oahu, Hawaii, USA. J. Sediment. Res. 74, 49–63. https://doi.org/10.1306/070203740049.

Grossman, E., Barnhardt, W., Hart, P., Richmond, B., Field, M., 2006. Shelf stratigraphy and the influence of antecedent substrate on Holocene reef development, south Oahu, Hawaii. Mar. Geol. 226, 97–114. https://doi.org/10.1016/j.margeo.2005.09.012.

Henson, F., 1950. Cretaceous and Tertiary reef formations and associated sediments in Middle East. AAPG Bull. 34, 215–238. https://doi.org/10.1306/3D933ED2-16B1-11D7-8645000102C1865D.

Hongo, C., 2012. Holocene key coral species in the Northwest Pacific: indicators of reef formation and reef ecosystem responses to global climate change and anthropogenic stresses in the near future. Quat. Sci. Rev. 35, 82–99. https://doi.org/10.1016/j.quascirev.2012.01.011.

Hongo, C., Kayanne, H., 2010. Holocene sea-level record from corals: reliability of paleodepth indicators at Ishigaki Island, Ryukyu Islands, Japan. Palaeogeogr. Palaeoclimatol. Palaeoecol. 287, 143–151. https://doi.org/10.1016/j.palaeo.2010.01.033.

Horton, B.P., Gibbard, P.L., Milne, G.M., Morley, R.J., Purintavaragul, C., Stargardt, J.M., 2005. Holocene sea levels and palaeoenvironments, Malay-Thai Peninsula, southeast Asia. The Holocene 15, 1199–1213. https://doi.org/10.1191/0959683605hl891rp.

Huang, D.Y., Shi, Q., Zhang, Y.C., 2005. The coral reef and high sea level in Luhuitou, Hainan Island during Holocene. Mar. Geol. Quat. Geol. 25, 1–7.

Huang, H., Qiu, X., Xu, Y., Zeng, G., 2011a. Crustal structure beneath the Xisha Islands of the South China Sea simulated by the teleseismic receiver function method. Chin. J. Geophys.-Chinese Edition 54, 2788–2798.

Huang, H., Qiu, X., Xu, H., Zhao, M., Hao, T., Xu, Y., Li, J., 2011b. Preliminary results of the earthquake observation and the onshore-offshore seismic experiments on Xisha Block. Chin. J. Geophys.-Chinese Edition 54, 3161–3170. https://doi.org/10.1002/cjg2.1683.

Jiang, W., Yu, K., Fan, T., Xu, S., Wang, R., Zhang, Y., Yue, Y., Zhao, J., Feng, Y., Wei, C., Wang, S., Wang, Y., 2019. Coral reef carbonate record of the Pliocene-Pleistocene climate transition from an atoll in the South China. Mar. Geol. 411, 88–97. https://doi.org/10.1016/j.margeo.2019.02.006.

Jiang, L., Yu, K., Tao, S., Wang, S., Han, T., Jiang, W., 2021. ENSO variability during the medieval climate anomaly as recorded by porites corals from the northern South China Sea. Paleoceanogr. Paleoclimatol. 36, e2020PA004173 https://doi.org/10.1029/2020PA004173.

Johnson, D., Risk, M., 1987. Fringing reef growth on a terrigenous mud foundation, Fantome Island, central Great Barrier Reef, Australia. Sedimentology 34, 275–287. https://doi.org/10.1111/j.1365-3091.1987.tb00777.x.

Kench, P.S., Brander, R.W., 2006. Wave processes on coral reef flats: implications for reef geomorphology using Australian case studies. J. Coast. Res. 22, 209–223. https://doi.org/10.2112/05A-0016.1.

Kench, P.S., Smithers, S.G., Mclean, R.F., Nichol, S.L., 2009. Holocene reef growth in the Maldives: Evidence of a mid-Holocene sea-level highstand in the central Indian Ocean. Geology 37, 455–458. https://doi.org/10.1130/G25590A.1.

Kennedy, D., Woodroffe, C., 2000. Holocene lagoonal sedimentation at the latitudinal limits of reef growth, Lord Howe Island, Tasman Sea. Mar. Geol. 169, 287–304. https://doi.org/10.1016/S0025-3227(00)00093-1.

Khan, N.S., Ashe, E., Shaw, T.A., Vacchi, M., Walker, J., Peltier, W.R., Kopp, R.E., Horton, B.P., 2015. Holocene relative sea-level changes from near-, intermediate-, and far-field locations. Curr. Clim. Change Rep. 1, 247–262. https://doi.org/10.1007/s40641-015-0029-z.

Khan, N.S., Ashe, E., Horton, B.P., Dutton, A., Kopp, R.E., Brocard, G., Engelhart, S.E., Hill, D.F., Peltier, W., Vane, C.H., 2017. Drivers of Holocene sea-level change in the Caribbean. Quat. Sci. Rev. 155, 13–36. https://doi.org/10.1016/j.quascirev.2016.08.032.

Lambeck, K., Rouby, H., Purcell, A., Sun, Y., Sambridge, M., 2014. Sea level and global ice volumes from the Last Glacial Maximum to the Holocene. Proc. Natl. Acad. Sci. 111, 15296–15303. https://doi.org/10.1073/pnas.1411762111.

Leonard, N., Welsh, K., Zhao, J., Nothdurft, L., Webb, G., Major, J., Feng, Y., Price, G., 2013. Mid-Holocene sea-level and coral reef demise: U-Th dating of subfossil corals in Moreton Bay, Australia. The Holocene 23, 1841–1852. https://doi.org/10.1177/0959683613508156.

Leonard, N., Welsh, K., Clark, T., Feng, Y., Pandolfi, J., Zhao, J., 2018. New evidence for "far-field" Holocene sea level oscillations and links to global climate records. Earth Planet. Sci. Lett. 487, 67–73. https://doi.org/10.1016/j.epsl.2018.02.008.

Leonard, N., Lepore, M., Zhao, J., Rodriguez-Ramirez, A., Butler, I., Clark, T., Roff, G., McCook, L., Nguyen, A., Feng, Y., Pandolfi, J., 2020. A U-Th dating approach to understanding past coral reef dynamics and geomorphological constraints on future reef growth potential; Mazie Bay, Southern Great Barrier Reef. Paleoceanogr. Paleoclimatol. 35, e2019PA003768 https://doi.org/10.1029/2019PA003768.

Lu, Y., Yang, X., Jia, R., 1979. Quarternary biological sediments in the Xisha Archipelago, China and a discussion on the age of island-formation. Geochimica 2, 93–104, 10. 19700/j. 0379-1726. 1979. 02. 001.

Luo, W., Wenyan, H.U., Wang, Y., Weijun, H.E., Jiao, X., Zhang, J., 2018. Characteristics of main reef-building organisms in Well XK-1, Xisha Islands and implications for environmental evolution. Mar. Geol. Quat. Geol. 38, 78–90. https://doi.org/10.16562/j.cnki.0256-1492.2018.06.008.

Macintyre, I., Glynn, P., Cortés, J., 1992. Holocene reef history in the eastern Pacific: mainland Costa Rica, Caño Island, Cocos Island, and Galápagos Islands. Proc. 7th Int. Coral Reef Symp. Guam 2, 1174–1184.

Majewski, J.M., Switzer, A.D., Meltzner, A.J., Parham, P.R., Horton, B.P., Bradley, S.L., Pile, J., Chiang, H.-W., Wang, X., Ng, C.T., 2018. Holocene relative sea-level records from coral microatolls in Western Borneo, South China Sea. The Holocene 28, 1431–1442. https://doi.org/10.1177/0959683618777061.

Mann, T., Bender, M., Lorscheid, T., Stocchi, P., Vacchi, M., Switzer, A., Rovere, A., 2019. Holocene sea levels in Southeast Asia, Maldives, India and Sri Lanka: the SEAMIS database. Quat. Sci. Rev. 219, 112–125. https://doi.org/10.1016/j.quascirev.2019.07.007.

Marshall, J., Davies, P., 1982. Internal structure and Holocene evolution of one tree reef, southern great barrier reef. Coral Reefs 1, 21–28. https://doi.org/10.1007/BF00286536.

McManus, J., Anderson, R., Broecker, W., Fleisher, M., Higgins, S., 1998. Radiometrically determined sedimentary fluxes in the sub-polar North Atlantic during the last 140,000 years. Earth Planet. Sci. Lett. 155, 29–43. https://doi.org/10.1016/S0012-821X(97)00201-X.

Meltzner, A., Switzer, A., Horton, B., Ashe, E., Qiu, Q., Hill, D., Bradley, S., Kopp, R., Hill, E., Majewski, J., 2017. Half-metre sea-level fluctuations on centennial timescales from mid-Holocene corals of Southeast Asia. Nat. Commun. 8, 1–16. https://doi.org/10.1038/ncomms14387.

Milne, G., Long, A., Basdett, S., 2005. Modelling Holocene relative sea-level observations from the Caribbean and South America. Quat. Sci. Rev. 24 (10–11), 1183–1202. https://doi.org/10.1016/j.quascirev.2004.10.005.

Mitrovica, J.X., Milne, G.A., 2002. On the origin of late Holocene sea-level highstands within equatorial ocean basins. Quat. ence Rev. 21, 2179–2190. https://doi.org/10.1016/S0277-3791(02)00080-X.

Montaggioni, L.F., 1988. Holocene reef growth history in mid-plate high volcanic islands. Proc. Sixth Int. Coral Reef Symp. Townsville 3, 455–460.

Montaggioni, L.F., 2005. History of Indo-Pacific coral reef systems since the last glaciation: development patterns and controlling factors. Earth Sci. Rev. 71, 1–75. https://doi.org/10.1016/j.earscirev.2005.01.002.

Nie, B., 1996. Sea-level changes of the South China Sea in the past 5000 years. Quat. Sci. 1, 80–87.

Peltier, W., Argus, D.F., Drummond, R., 2018. Comment on "An assessment of the ICE-6G_C (VM5a) glacial isostatic adjustment model" by Purcell et al. J. Geophys. Res. Solid Earth 123, 2019–2028. https://doi.org/10.1002/2016JB013844.

Perry, C., Smithers, S., Roche, R., Wassenburg, J., 2011. Recurrent patterns of coral community and sediment facies development through successive phases of Holocene inner-shelf reef growth and decline. Mar. Geol. 289, 60–71. https://doi.org/10.1016/j.margeo.2011.09.012.

Pirazzoli, P., Montaggioni, L., Vergnaud-Grazzini, C., Saliege, J., 1987. Late Holocene sea levels and coral reef development in Vahitahi Atoll, eastern Tuamotu Islands, Pacific Ocean. Mar. Geol. 76, 105–116.

Qin, Yeman, Yu, Kefu, Wang, Rui, Wei, Jiang, Xu, Shendong, 2019. The Initiation Time of the Holocene Coral Reef at the Chenhang Island (Xisha Islands) and Its Significance as a Sea Level Indicator. Trop. Geogr. 39 (3), 319–328.

Rees, S., Opdyke, B., Wilson, P., Fifield, L., Levchenko, V., 2006. Holocene evolution of the granite based Lizard Island and MacGillivray reef systems, Northern Great Barrier Reef. Coral Reefs 25, 555–565. https://doi.org/10.1007/s00338-006-0138-1.

Roy, K., Peltier, W., 2015. Glacial isostatic adjustment, relative sea level history and mantle viscosity: reconciling relative sea level model predictions for the US East coast with geological constraints. Geophys. J. Int. 201, 1156–1181. https://doi.org/10.1093/gji/ggv066.

Roy, K., Peltier, W., 2017. Space-geodetic and water level gauge constraints on continental uplift and tilting over North America: regional convergence of the ICE-6G_C (VM5a/VM6) models. Geophys. J. Int. 210, 1115–1142. https://doi.org/10.1093/gji/ggx156.

Sanborn, K., Webster, J., Webb, G., Braga, J., Humblet, M., Nothdurft, L., Patterson, M., Dechnik, B., Warner, S., Graham, T., 2020. A new model of Holocene reef initiation and growth in response to sea-level rise on the Southern Great Barrier Reef. Sediment. Geol. 397, 105556. https://doi.org/10.1016/j.sedgeo.2019.105556.

Saunders, M., Albert, S., Roelfsema, C., Leon, J., Woodroffe, C., Phinn, S., Mumby, P., 2016. Tectonic subsidence provides insight into possible coral reef futures under rapid sea-level rise. Coral Reefs 35, 155–167. https://doi.org/10.1007/s00338-015-1365-0.

Shao, L., Li, Q., Zhu, W., Zhang, D., Qiao, P., Liu, X., You, L., Cui, Y., Dong, X., 2017. Neogene carbonate platform development in the NW South China Sea: Litho-, bio- and chemo-stratigraphic evidence. Mar. Geol. 385, 233–243. https://doi.org/10.1016/j.margeo.2017.01.009.

Shen, C., Li, K., Sieh, K., Natawidjaja, D., Cheng, H., Wang, X., Edwards, R., Lam, D., Hsieh, Y., Fan, T., 2008. Variation of initial 230Th/232Th and limits of high precision U–Th dating of shallow-water corals. Geochim. Cosmochim. Acta 72, 4201–4223. https://doi.org/10.1016/j.gca.2008.06.011.

Shi, X., Yu, K., Chen, T., 2007. Progress in researches on sea-level changes in South China Sea since mid-Holocene. Mar. Geol. Quat. Geol. 27, 121–132. https://doi.org/10.16562/j. cnki. 0256–1492. 2007. 05. 003.

Shi, X., Yu, K., Chen, T., Zhang, R., Zhao, J., 2008. Mid-to late-Holocene sea level highstands: Evidence from fringing coral reefs at Qionghai, Hainan Island. Marine Geology & Quaternary Geology 28, 1–9. https://doi.org/10.3724/SP.J.1140.2008.050.

Smith, D.E., Harrison, S., Firth, C.R., Jordan, J.T., 2011. The early Holocene sea level rise. Quat. Sci. Rev. 30, 1846–1860. https://doi.org/10.1016/j.quascirev.2011.04.019.

Smithers, S., Hopley, D., Parnell, K., 2006. Fringing and nearshore coral reefs of the Great Barrier Reef: episodic Holocene development and future prospects. J. Coast. Res. 22, 175–187. https://doi.org/10.2112/05A-0013.1.

Thompson, W., Spiegelman, M., Goldstein, S., Speed, R., 2003. An open-system model for U-series age determinations of fossil corals. Earth Planet. Sci. Lett. 210, 365–381. https://doi.org/10.1016/S0012-821X(03)00121-3.

Toscano, M.A., Gonzalez, J.L., Whelan, K.R., 2018. Calibrated density profiles of Caribbean mangrove peat sequences from computed tomography for assessment of peat preservation, compaction, and impacts on sea-level reconstructions. Quat. Res. 89, 201. https://doi.org/10.1017/qua.2017.101.

Toth, L.T., Macintyre, I.G., Aronson, R.B., 2017. Holocene Reef Development in the Eastern Tropical Pacific. In: Glynn, P., Manzello, D., Enochs, I. (Eds.), Coral Reefs of the Eastern Tropical Pacific. Coral Reefs of the World, Vol 8. Springer, Dordrecht. https://doi.org/10.1007/978-94-017-7499-46.

Wan, J.X.W., Meltzner, A.J., Switzer, A.D., Lin, K., Wang, X., Bradley, S.L., Natawidjaja, D.H., Suwargadi, B.W., Horton, B.P., 2020. Relative sea-level stability and the radiocarbon marine reservoir correction at Natuna Island, Indonesia, since 6400 yr BP. Mar. Geol. 430, 106342. https://doi.org/10.1016/j.margeo.2020.106342.

Wang, G., Lu, B., Quan, S., 1982. The fundamental sedimentary facies of modern coral reefs in Hainan and Xisha islands. Oil Gas Geol. 3, 211–223.

Wang, R., Yu, K., Jones, B., Wang, Y., Zhao, J., Feng, Y., Bian, L., Xu, S., Fan, T., Jiang, W., 2018. Evolution and development of Miocene "island dolostones" on Xisha Islands, South China Sea. Mar. Geol. 406, 142–158. https://doi.org/10.1016/j.margeo.2018.09.006.

Webb, A., Kench, P., 2010. The dynamic response of reef islands to sea-level rise: evidence from multi-decadal analysis of island change in the Central Pacific. Glob. Planet. Chang. 72, 234–246. https://doi.org/10.1016/j.gloplacha.2010.05.003.

Woodroffe, S.A., Horton, B.P., 2005. Holocene sea-level changes in the Indo-Pacific. J. Asian Earth Sci. 25, 29–43. https://doi.org/10.1016/j.jseaes.2004.01.009.

Woodroffe, C., Webster, J., 2014. Coral reefs and sea-level change. Mar. Geol. 352, 248–267. https://doi.org/10.1016/j.margeo.2013.12.006.

Woodroffe, C., Beech, M., Gagan, M., 2003. Mid-late Holocene El Niño variability in the equatorial Pacific from coral microatolls. Geophys. Res. Lett. 30 (7), 1358. https://doi.org/10.1029/2002GL015868.

Xu, S., Yu, K., Fan, T., Jiang, W., Wang, R., Zhang, Y., Yue, Y., Wang, S., 2019. Coral reef carbonate $\delta^{13}C$ records from the northern South China Sea: A useful proxy for seawater $\delta^{13}C$ and the carbon cycle over the past 1.8 Ma. Glob. Planet. Chang. 182, 103003. https://doi.org/10.1016/j.gloplacha.2019.103003.

Yamano, H., Inoue, T., Adachi, H., Tsukaya, K., Adachi, R., Baba, S., 2019. Holocene sea-level change and evolution of a mixed coral reef and mangrove system at Iriomote Island, southwest Japan. Estuar. Coast. Shelf Sci. 220, 166–175. https://doi.org/10.1016/j.ecss.2019.03.001.

Yu, K., Zhao, J., 2009. Coral reefs (of the South China Sea). In: Wang, P.X., Li, Q.Y. (Eds.), The South China Sea-Paleoceanography and sedimentology. Springer, Dordrecht, The Netherlands, pp. 186–209.

Yu, K., Zhao, J., 2010. U-series dates of Great Barrier Reef corals suggest at least +0.7 m sea level ~7000 years ago. The Holocene 20, 161–168. https://doi.org/10.1177/0959683609350387.

Yu, K., Zhong, J., Zhao, J., Shen, C., Chen, T., Liu, T., 2002. Biological-geomorphological zones in a coral reef area at southwest Leizhou Peninsula unveil multiple sea level high-stands in the Holocene. Mar. Geol. Quat. Geol. 22, 27–32.

Yu, K., Zhao, J., Shi, Q., Chen, T., Wang, P., Collerson, K., Liu, T., 2006. U-series dating of dead Porites corals in the South China Sea: evidence for episodic coral mortality over the past two centuries. Quat. Geochronol. 1, 129–141. https://doi.org/10.1016/j.quageo.2006.06.005.

Yu, K., Zhao, J., Done, T., Chen, T., 2009. Microatoll record for large century-scale sea-level fluctuations in the mid-Holocene. Quat. Res. 71, 354–360. https://doi.org/10.1016/j.yqres.2009.02.003.

Yu, K., Zhao, J., Lawrence, M., Feng, Y., 2010. Timing and duration of growth hiatuses in mid Holocene massive Porites corals from the northern South China Sea. J. Quat. Sci. 25, 1284–1292. https://doi.org/10.1002/jqs.1410.

Zhang, Y., Yu, K., Qian, H., Fan, T., Yue, Y., Wang, R., Jiang, W., Xu, S., Wang, Y., 2020. The basement and volcanic activities of the Xisha Islands: Evidence from the kilometre-scale drilling in the northwestern South China Sea. Geol. J. 55, 571–583. https://doi.org/10.1002/gj.3416.

Zhao, H., 1998. Characteristics of Neotectonic Movement of Coral Reef Area of the South China Sea Islands. Marine Geology and Quaternary Geology/Haiyang Dizhi Yu Disiji Dizhi. Qingdao, 18, pp. 37–45.

Zhao, J., Yu, K., 2002. Timing of Holocene sea-level highstands by mass spectrometric U-series ages of a coral reef from Leizhou Peninsula, South China Sea. Chin. Sci. Bull. 47, 348–352. https://doi.org/10.1007/BF02901194.

Zhao, H.T., Zhang, Q.M., Song, C.J., Qiu, Z., Lin, X., Yuan, J., 1999. Geomorphology and environment of the south China coast and the South China Sea islands (in Chinese). Science Press, Beijing, p. 221.

Zhao, M., Yu, K., Shi, Q., Yang, H., Riegl, B., Zhang, Q., Yan, H., Chen, T., Liu, G., Lin, Z., 2017. Comparison of coral diversity between big and small atolls: a case study of Yongle atoll and Lingyang reef, Xisha Islands, central of South China Sea. Biodivers. Conserv. 26, 1143–1159. https://doi.org/10.1007/s10531-017-1290-3.

Zong, Y., 2004. Mid-Holocene sea-level highstand along the Southeast Coast of China. Quat. Int. 117, 55–67. https://doi.org/10.1016/S1040-6182(03)00116-2.